

PAPER

High accuracy characterisation for the absolute energy of scandium $K\alpha$

To cite this article: J W Dean *et al* 2019 *J. Phys. B: At. Mol. Opt. Phys.* **52** 165002

View the [article online](#) for updates and enhancements.



IOP | ebooksTM

Bringing you innovative digital publishing with leading voices to create your essential collection of books in STEM research.

Start exploring the collection - download the first chapter of every title for free.

High accuracy characterisation for the absolute energy of scandium $K\alpha$

J W Dean, H A Melia, C T Chantler¹  and L F Smale

School of Physics, The University of Melbourne, Melbourne, Australia

E-mail: jonathan.dean@unimelb.edu.au, h.melia@student.unimelb.edu.au, chantler@unimelb.edu.au and lucas.smale@gmail.com

Received 4 March 2019, revised 17 May 2019

Accepted for publication 13 June 2019

Published 24 July 2019



CrossMark

Abstract

This work reports the absolute characterisation of the Sc $K\alpha$ profile. All component peaks are characterised for the first time. The satellite component centroids, line-widths, and relative intensities are determined. Energies are calibrated on an absolute basis. Sc $K\alpha_1^0$ and $K\alpha_2^0$ peak energies of 4090.699(10) eV and 4085.926(18) eV are reported, respectively, with estimated standard error uncertainties of 2.4 and 4.4 ppm. In this work, an electron gun operating at 20 kV, incident on high purity metals, produces the x-ray fluorescence, which Bragg diffracts via a Germanium (220) crystal to permit high-accuracy measurement of energy. The $K\alpha$ emission spectrum of scandium ($Z = 21$) has not been measured in absolute energy in over 50 years. At the time the data was reported in 'x units' and the angstrom was not a well defined unit. That reported uncertainty was estimated to be approximately 50 ppm (parts per million) or 0.2 eV. The new profile characterisation combined with the absolute energy calibration provides an important definition for future studies in chemical speciation and condensed matter studies. Furthermore, the methodology described obtains a level of accuracy from relatively low energy x-rays to provide an important insight for future studies in fundamental parameters, pionic spectra and high-accuracy tests of QED.

Keywords: scandium, characteristic radiation, K alpha, x-ray spectroscopy, absolute measurement, 2–4 parts per million

(Some figures may appear in colour only in the online journal)

1. Introduction

Understanding characteristic x-ray radiation spectra has been a major topic in atomic physics research from the first analysis by Barkla in 1909 and for many decades [1, 2]. In this international year of the periodic table of the elements it is important to remember that the definition of the periodic table, based on the characteristic radiation of x-rays from elements and hence inner-shell atomic binding energies, was made by Moseley in 1913 [3] and that anomalous and asymmetric shapes were reported in 1933 [4, 5]. Indeed atomic physics laid the foundation for quantum theory, relativistic quantum mechanics (QM) and quantum electrodynamics (QED) in the first half of the last century. Anomalies in the literature for fundamental atomic and exotic

systems (hydrogen, muonic hydrogen, muonic deuterium, pionic atoms and medium- Z few-electron systems [6–10]) are some of the cutting edges of theory and experiment today. These depend upon a critical understanding, a new understanding, of fundamental parameters [11]. Fundamental parameters include transition probabilities, experimental line strengths and spectral components, atomic edge profiles and especially the characteristic radiation viz the $K\alpha$ and $K\beta$ spectra of critical elements of the periodic table [12, 13]. The understanding of fundamental parameters is a critical drive today for industrial funding and support, perhaps especially in Europe, because of the key insight which can ensue for industrial and scientific purposes from well-defined and well-understood calibration and characterisation of instruments. Whilst some modern research in atomic physics have just assumed or depended upon the fundamental characterisation

¹ Author to whom any correspondence should be addressed.

of earlier workers and standards laboratories, these remain the core drivers of scientific and industrial endeavour.

X-ray characteristic spectra offer insight into complex inner-shell interactions of electrons, have application to chemistry [14], astrophysics [15], plasma physics [16], nanopowders [17] and medicine [18], and have the potential to test fundamental constraints on QED [8, 19–21]. For example, the current two highest accuracy characterisations of Cu $K\alpha$ reveal differences of 12 standard errors and demand further detailed investigation [2, 22–24]; the anomalies in exotic and few-electron spectra demand high-accuracy calibration techniques down to 1 part per million [8]; and the complex pattern of discrepancy of spectra from theory in the transition metals in particular demands new careful scrutiny across the sequence [25, 26].

The absolute energy profile for scandium has not been experimentally obtained in over 50 years, since Bearden [1]. Relative measurements of energy have been performed for scandium [27–31] involving investigations into phenomena such as the anomalous Z -dependence of the $K\alpha$ line strengths, anomalous asymmetries, and chemical shifts. These investigations present absolute energy on the x -axis by calibrating the $K\alpha_1$ and $K\alpha_2$ peaks to the results by Bearden [1].

The $2p_{3/2}$ state has double the degeneracy of the $2p_{1/2}$. This suggests that the ratio of the integrated intensity of the peaks: $I(K\alpha_1): I(K\alpha_2)$ should be exactly 0.5. Experimentally, and shown in relativistic QM, this ratio increases with atomic number [22, 32, 33]. This anomalous Z -dependence, and the anomalous asymmetry, are of particular importance across the 3d transition metals ($Z = 21$ to $Z = 30$) because the 3d electrons in particular contribute to the amplitudes and structure in the spectra [34].

Shake processes are the favoured explanation of additional satellite components, non-degenerate to the diagram components, which give rise to the asymmetries [31, 35, 36]. Shake processes occur when an extra electron is excited into a higher shell (shake-up) or into the continuum (shake-off), the transition then takes place in a different potential due to the spectator vacancy.

As the fine structure splitting of the $2p$ shell is a relativistic phenomenon, it scales with Z . Because scandium is the lowest Z transition metal, resolving the $K\alpha_{1,2}$ lines becomes more challenging. A relatively low $K\alpha$ energy also poses some challenges for x-ray diffraction. The analytic methodology of this work pave the way for high accuracy measurements of energy. These methods can be extended to tests for QED anomalies, such as in the He-like Ti spectra [37].

Absolute measurement of the energy scale in x-ray experiments is calibrated by the lattice spacing of silicon or germanium, using the x-ray and optical interferometer and δ -D instruments, usually at a standards laboratory [11, 13, 38–40]; or relative to thus-calibrated edge energies with some difficulty in cross-platform independence and hence accuracy, often at synchrotrons; or relative to thus-calibrated characteristic energies, at laboratory and exotic sources. A relative measurement by contrast is not calibrated to the experimental chain to the metre or frequency, and is instead either pinned to

a theoretical computation or may be directly on a relative scale of energy with possible offset and scale uncertainties of indeterminate magnitude [2, 24].

The approach using a diffracting crystal with known lattice spacing is particularly sensitive to thermal expansion, high-level interferometry, crystal strain and source location. These issues can be accounted for, such as in the recent work [23], requiring extensive run time and financial cost. The current method in this work extends that done before for absolute measurement of x-ray spectra by calibrating the energy scale using independently known and measured, experimentally robust x-ray transitions. Any uncertainty from the reference transitions must be included in our final uncertainty, together with uncertainties of our measurement of these same spectra. The basic method has been used before in numerous previous experiments [8, 41, 42]. Many past measurements have used the peak spectral locations $K\alpha_1^0$ and $K\alpha_2^0$ and possibly $K\beta_{13}^0$ to define the energy calibration. Bearden and others defined these as the observed spectral peak of the experimental spectrum, possibly fitted with a local quadratic function [1]. Whilst this is useful, it has large uncertainties from changes of resolution and hence energy from one experimental setup compared with for example the reference energy peak determination. Hence we discuss and present the methodology for accurate transfers using the whole reference spectra and characterisations which can attain a much improved accuracy. Here we develop the curved crystal diffraction approach and apply it using a laboratory experimental set-up to scandium.

There is a large gap in the literature in experiment in the region of scandium characteristic radiation and below in energy, in part because of the challenging experimental regime. We define the energies in a cross-platform independent manner relative to the SI units for the first time; and some 20 times more accurate than the previous claimed absolute measurement 50 years ago.

Theoretical calculations of the Sc $K\alpha$ energy spectrum are extremely complex due to the open shells, and the lone 3d electron. Recent theoretical calculations involve multi-configurational Dirac Hartree–Fock (MCDHF) methods [13, 43]. Comparing theory to the previous absolute energy measurement gives no insight into current relativistic QM calculations. However, this new measurement, with uncertainties at the 2–4 ppm level, permits novel insight for and from MCDHF calculations. This gives two examples of fundamental parameter investigations and high-accuracy experimental measurement providing new opportunities and tools for experimental and theoretical atomic physics development.

This work provides a high-accuracy absolute measurement of the Sc $K\alpha$ profile, component energies and parameters and the determined peak values Sc $K\alpha_1^0$, Sc $K\alpha_2^0$, filling a major gap in the current atomic physics literature, with standard error uncertainties of 2.4 and 4.4 ppm, some 20 times more accurate than the previous work. It compares results to past observations and measurements, and provides high-accuracy data towards the investigation of current challenges in x-ray characteristic radiation. It also presents a

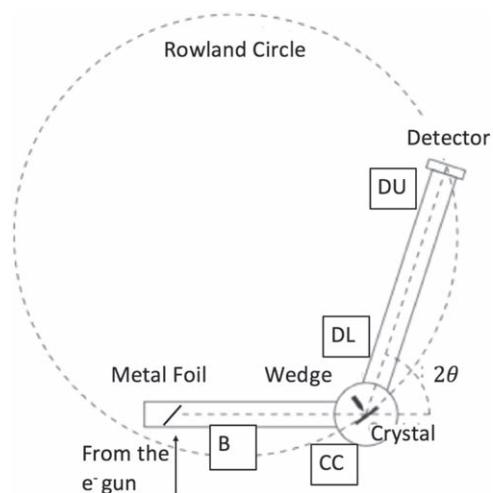


Figure 1. A schematic diagram of the experimental set-up with the clinometers labels in boxes at their approximate position in the experimental set-up. Each clinometer measures the angle of the arm or crystal relative to the local direction of gravity (i.e. down in the figure).

methodology newly applied to laboratory spectroscopy with a new approach and analysis for vignetting and other experimental systematics.

2. Experimental setup

An electron gun bombards high purity (>99.99% by mass) samples of elements $Z = 21$ (scandium) and $Z = 22$ to $Z = 25$ (for calibration) in turn to generate the x-ray source. The energy of the electron gun (20 keV) ensures that K -transitions are recorded and stable, towards the sudden impact limit. The electrons are incident on the metal surface at 45° to maximise the photons propagated towards the monochromator, at an angle normal to the electron gun. The photons are Bragg diffracted by the Germanium (220) curved crystal monochromator (manufactured and calibrated by the National Institute of Standards and Technology) towards the detector arm, which is set at a Bragg angle of 2θ for the relevant spectrum. Three clinometers give raw output in voltage with reference to the base (B) clinometer, these were placed at the crystal housing (CC) and at the lower (DL) and upper (DU) portions of the detector arm, shown in figure 1.

The curved crystal has radius of curvature such that the Bragg angle for Ti $K\alpha$ (43.4°) diffraction places the detector on the Rowland circle ensuring focus of the most relevant calibration spectra for this measurement. Diffraction of low energy x-rays from Sc $K\alpha$ can lead to significant broadening. Having the curved crystal focused on Ti $K\alpha$ enables focused data for scandium, and offers a large set of focused calibration transitions for good statistics. Beyond the energy of Mn $K\beta$ the spectra recorded would be too defocused by the diffractometer point spread function (PSF) at the detector location (over 30 cm from the Rowland circle). Lower atomic numbers provide x-ray energies too low for a sharp diffraction profiles, and indeed, calcium ($Z = 20$) has a $K\alpha$ energy

uncertainty of roughly 100 ppm which is too large to be used as a calibration.

Also seen in figure 1 is an adjustable ‘Seeman’ wedge, which limits the diffracting region of the crystal, which in turn can alter bandpass, instrumental broadening (vignetting) and other complex systematics. The narrower the wedge, the more parallel the incident photon field, enabling the detector to be further from the Rowland circle with similar resolution. This is essential for transitions further away in energy from Ti $K\alpha$. However, too narrow a wedge leads to significant vignetting of the profile, when the spectrum is not a direct convolution of the spectrometer and detector PSF but instead is truncated to one side. This is a systematic that is dealt with in this work and leads to the final uncertainty reported a factor of 3 lower than if uncharacterised.

Peak energies, labelled $K\alpha_1^0$, $K\alpha_2^0$, $K\beta^0$, defined in any manner, are in no way sufficient to generate an accurate dispersion function, because the peak energy is not transferable and depends upon instrumental broadening well above the required accuracy [11, 23]. Rather the full component characterisation of each spectrum must be used. For this purpose, we use the component characterisation from Chantler *et al* [29], enabling us to use a consistent 6 Voigt characterisation for each profile. The full characterisation of the calibration profiles $Z = 22 \rightarrow Z = 25$ are given in table 1 of [29] along with the uncertainty in each value that we include and carry into our dispersion fit. The satellite structure of the Cu profile has been shown to be stable at and above an accelerating voltage of 20 kV [24]. Ergo, the calibration profiles are stable and consistent with our measurement as they are all measured ≥ 20 kV. See also [11]. The uncertainties of each experimental measurement of a calibration profile and characterisation, together with the uncertainties of the reference calibration characterisation, are all included in the analysis below. Many of these are of order 1–2 parts per million and they add according to the covariance matrix for extracting the Sc $K\alpha$ spectral profiles and component uncertainties.

The pressure inside the spectrometer (from calibration source to crystal, and crystal to detector) is less than 10^{-7} Torr. Figure 1 shows a diagram of the set-up with the target element (calibration source), 2θ angle of the arm, Seemann wedge, clinometers and detector.

Our backgammon two-dimensional ion chamber x-ray detector was filled with P10 (10% methane in argon) gas at approximately 1060 Torr (slightly above atmospheric pressure). The value of backgammon detectors has been discussed [44–50]. Our backgammon active area is about $22 \text{ mm} \times 22 \text{ mm}$. In the active width, this corresponds (in the spectrometer) to approximately 100 eV depending upon crystal angle, curvature and detector distance; detector processing yields a regional nonlinearity of order $1 \mu\text{m}$ and hence an accuracy in energy to below 1 ppm (part per million). Backgammon detectors have advantages of compactness, price, and portability, together with good spatial resolution and excellent linearity. The capacity to change the gas and gas pressure is a major advantage at lower energies where the absorption coefficient becomes large [50].

Table 1. Key parameters of the experimental setup with estimated uncertainties.

Name	Symbol	Value	Estimated 1σ uncertainty
Rowland circle radius	R_z	1121 mm	10 mm
Detector arm length	ZF	1500 mm	5 mm
Source to crystal length	BX_z	330 mm	5 mm
Source FWHM	sw	5 mm	1 mm
Crystal thickness	T	0.820 mm	0.005 mm

Electron output shape: Gaussian with FWHM 5 mm
 Three wedge gaps (figure 1): 2.54(1) mm, 4.58(1) mm, and 14.00 (1) mm (fully open)

Key parameters for the x-ray optical geometry are outlined in table 1. Symbols are consistent with [51], figure 2.

3. Data collection

For each $K\alpha$ and $K\beta$ transition, 3 runs were performed at each of three different wedge positions (2.54, 4.98, 14.00 mm). Run times are roughly 20 min each to give the order of 10^4 counts at the peak of the spectra. For each run, the detector arm was shifted slightly so the spectra would be incident on different positions along the detector face: one reading near the centre of the detector face, and one slightly to the left and right, at typically ± 1 mm. This helps in mapping the dispersion function calibration of the clinometers and in the calibration of the 2θ angle; in identifying vignetted spectra; and to account for electromagnetic edge effects [50].

Figure 2 illustrates one of the Cr $K\alpha$ calibration profiles. This is not near the region of Ti $K\alpha$ and therefore not ideally focused, yet there is still excellent agreement between the model and the raw data. Some structure in the residual, especially around the maxima of each peak and the minima between the peaks, generally remains within \sqrt{N} , the one standard deviation uncertainty envelope. All previous work on the $K\alpha$ profiles of elements observe similar residual structure with similar χ_r^2 including on the much more well-resolved Cu $K\alpha$ spectrum (e.g. [23] figure 18).

4. Data analysis

The essence of this experiment is to calibrate the spectra to energy. This is done by using the calibration transitions to model a functional that takes clinometry voltage to angle, and curved crystal theory *Mosplate* to map energy to angle [51–53].

Mosplate diffraction phenomena include refractive index corrections, depth penetration of the wavefield into the crystal, and lateral shifts in position due to x-rays penetrating the crystal. For each energy, a range of spectra are calculated at different crystal angles. A peak position, X , on the detector

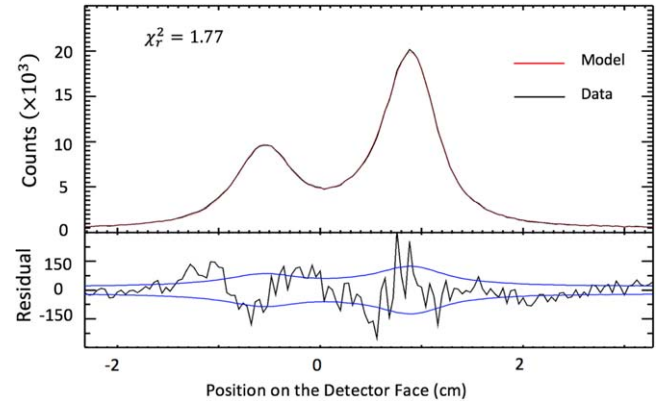


Figure 2. Raw data profile for a single calibration spectra and the model [22, 29] for Cr $K\alpha$, with residual. The χ_r^2 value shows the excellent agreement between experiment and model.

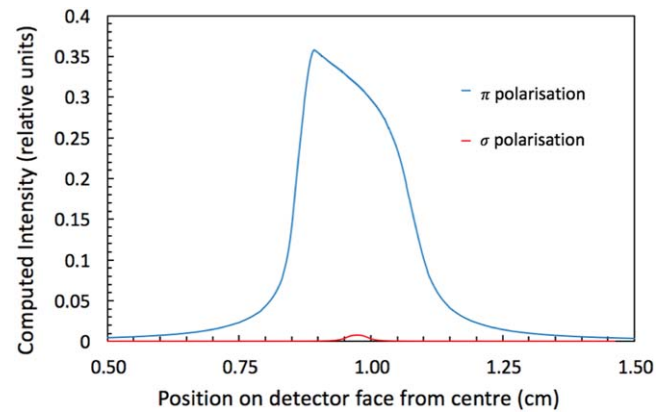


Figure 3. Theoretical diffraction profile as a function of position on the detector face calculated from *Mosplate* from π and σ polarised photons (at 4090.735 eV) with geometric inputs from table 1. The parallel polarised photons (σ) are heavily damped, as expected from a 45° diffracting angle.

face is then computed for each of these spectra as a function of E and θ : $X = X_{mos}(E, \theta)$. The model also defines inverse functions that calculate E and θ from the other variables: $E = E_{mos}(X, \theta)$ and $\theta = \theta_{mos}(E, X)$. Significant geometric parameters used by *Mosplate* are given in table 1. An example of the calculated diffraction curve is shown in figure 3.

Following the theoretical diffraction modelling, the clinometers are calibrated for angles and energies using K -transitions for elements $Z = 22$ to $Z = 25$ with their 6 Voigt characterisation in [29]. The position on the detector face, the energy of the profile, and the *Mosplate* equation $\theta = \theta_{mos}(X, E)$ are used to give an angle. The angle calibrates the clinometers using a functional $f_{disp}(V) = \theta$ for V , voltage. The absolute energy measurement for scandium can then be found by applying the dispersion function and using the *Mosplate* equation: $E = E_{mos}(X, f_{disp}(V))$. An example of the dispersion function is shown in figure 4. The one standard error uncertainty for the fit of the dispersion function is calculated from the fitted covariance matrix.

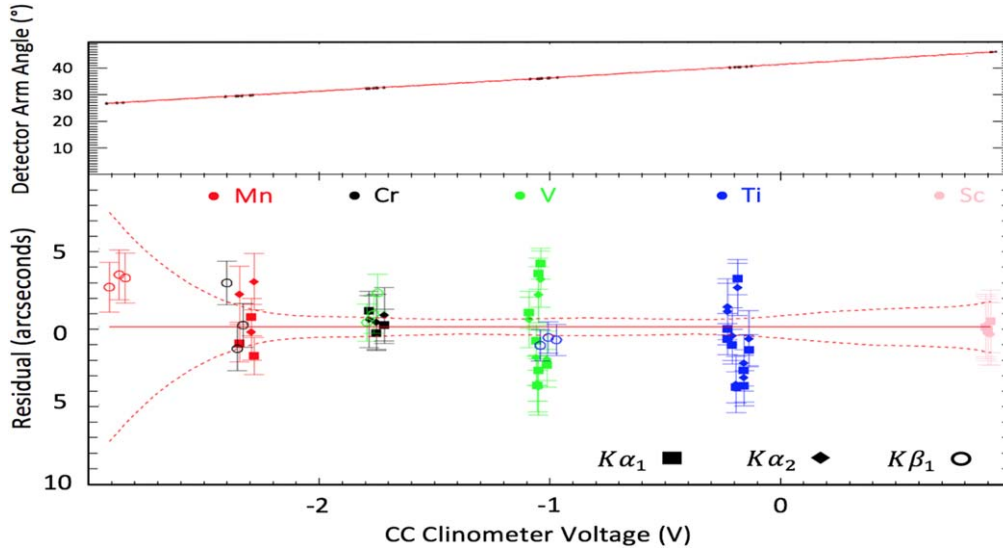


Figure 4. The dispersion function for one of the clinometers (CC). The residual red-dotted line shows the calculated one standard error uncertainty for the fit extrapolated to the region of Sc $K\alpha$ energies (see text). The upper plot looks ideal, but the lower expanded plot reveals structure and residuals of the modelling. The residual plot also shows the one standard error uncertainties in the position for each transition centroid. Most of the data points, with their individual fitting uncertainty, lie within the one standard error envelope.

4.1. Vignetting

Vignetting is a common issue with high-resolution spectra and occurs when a slit, or ‘Seeman’ wedge, is relatively narrow and blocks some of the photons which would be incident upon the diffracting crystal and would otherwise diffract to the detector. This will result in an observed energy separation of the $K\alpha$ components less than the true value. However, the rectangular slit (wedge) has a very simple transitional form from fully open to fully obstructing, which corresponds to a ramp or triangular function. Hence we apply a linear vignetting function to investigate and model any spectra which might be significantly affected by this.

This function was included in the overall fitting of the spectra as a product, corresponding to a non-uniform convolution function (see [appendix](#)). This gives significant improvements to the χ_r^2 measure, up to a factor of three. Furthermore, without the vignetting function correction, the overall fit of the dispersion function (figure 4) has a greater value for χ_r^2 and the range of the residuals is a factor of two larger for vignettted calibration lines. Without the model correction these lines can be excluded, of course, but a significant achievement of the modelling is that this procedure, including or excluding vignettted spectra, is robust down to below 3 parts per million (ppm).

For the larger wedge gaps (4.94 and 14.00 mm) vignetting was neither necessary nor observed, and implementing the vignetting functional fit had no effect on profile spectra or χ_r^2 . Furthermore, there was no vignetting for the $K\beta$ profiles as expected since they are narrower spectral profiles.

4.2. Error budget

Table 2 presents our final error budget from this experiment. Fitting used weighted least-squares, which in the context of the analysis is equivalent with likelihood estimates, with

Table 2. The error budget for reported Sc $K\alpha_1^0$ and $K\alpha_2^0$ values. The individual errors are summed in quadrature to arrive at the final error. The dispersion function uncertainty is dominated by the extrapolation uncertainty and includes the uncertainty in all the reference data (see [appendix](#)).

Error source	Estimated 1 standard error uncertainty in this experiment
Total Sc $K\alpha_1^0$	0.010 eV (2.5 ppm)
Total Sc $K\alpha_2^0$	0.018 eV (4.4 ppm)
Sc $K\alpha_1^0$ statistics	0.005 eV (1.2 ppm)
Sc $K\alpha_2^0$ statistics	0.016 eV (3.9 ppm)
Sc $K\alpha$ clinometer statistics	0.004 eV (1.0 ppm)
Fitting the dispersion function	0.006 eV (1.5 ppm)
Total geometry from:	0.0052 eV (1.3 ppm)
Rowland circle radius (R_z)	0.0031 eV
Detector arm length (ZF)	0.0038 eV
Source to crystal length (BX_z)	0.0015 eV
Wedge width	0.0009 eV
Source FWHM (sw)	0.0005 eV
Crystal thickness (T)	0.0004 eV

$\chi_r^2 \approx 1$ in all cases. Our definition of the peak values Sc $K\alpha_1^0$, Sc $K\alpha_2^0$, is given not by the raw data location nor by a quadratic fit to the experimental spectra, both of which are unreliable at about 1–2 channels or up to 0.25 eV due to statistical noise; but by the reconstructed theoretical profile from the sum of all spectral components including any uncertainty from the correlation matrix (see [appendix](#)). As such this will be subject to small variations from changes in

Table 3. For each of the 4 subsets used in calibrating the dispersion function, the final answer for values for the centroid for each component position for Sc $K\alpha$ are shown. Numbers in parentheses are one standard error uncertainties of the quoted value referring to the last digits.

Subset of spectra (no.)	Peak i	Centroid C_i , eV
All (54)	$K\alpha_1^0$	4090.699(10)
	$K\alpha_2^0$	4085.926(18)
All $K\alpha$ (42)	$K\alpha_1^0$	4090.705(15)
	$K\alpha_2^0$	4085.933(28)
All non-vignetted (12 $K\beta$ and 13 $K\alpha$)	$K\alpha_1^0$	4090.678(20)
	$K\alpha_2^0$	4085.897(33)
All $K\beta$ (12)	$K\alpha_1^0$	4090.785(45)
	$K\alpha_2^0$	4086.002(101)

resolution or instrument function, with an instrumental broadening indicated by the Gaussian FWHM of up to 1.8 eV. The widths and instrument function widths of other literature spectra are very similar.

Note that the statistics on the measurement of the unknown Sc profile and components, rows 4–6, are dominant, and the fitting the dispersion function, row 7, is a sum of all geometric and functional uncertainties including especially the reference calibration uncertainties and the measurement uncertainties of those calibration profile spectra and of the clinometry of those reference measurements. In the contribution to the dispersion function uncertainty, the extrapolation uncertainty is dominant as expected. Note however that this is quite a small extrapolation especially given the range of reference data collected. A total of 42 $K\alpha$ spectra were measured with clinometry from each of three clinometers for each spectrum, together with 12 $K\beta$ spectra and the unknown Sc $K\alpha$ spectra. A meticulous error calculation is given in [appendix](#).

4.3. Subset analysis (robustness) and consistency

To ensure that the effect of the vignetting profile or differences between $K\alpha$ and $K\beta$ characterisations do not affect our results, we obtain the Sc $K\alpha$ peak energies from four different calibration subsets. Table 3 provides the absolute energies for Sc $K\alpha_{1,2}^0$ for each of the calibration subsets with calculated uncertainty. The range in $K\alpha_1^0$ energy is 0.0047 eV and for $K\alpha_2^0$ is 0.029 eV.

The 3 clinometers and 3 separate scans of the Sc $K\alpha$ profile give nine different results. Remarkable consistency across the values are shown in figures 5, 6, with all values within one standard error of another.

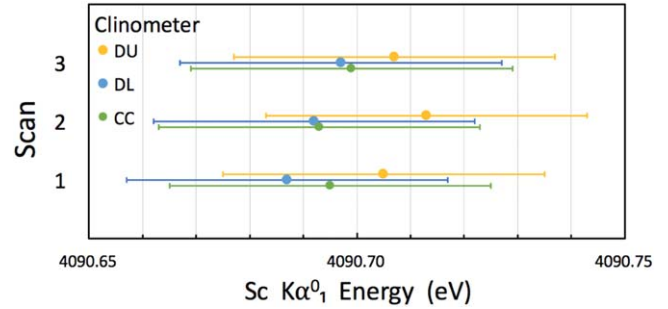


Figure 5. The values for the centroid of $K\alpha_1^0$ for each of the scans for each clinometer with its respective one standard error uncertainty. Individual uncertainties from statistics on profile, clinometry and dispersion mapping are 6–8 ppm.

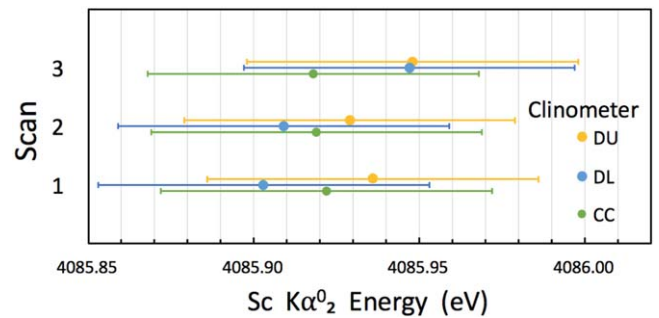


Figure 6. The values for the centroid of $K\alpha_2^0$ for each of the scans for each clinometer with its respective one standard error uncertainty. Individual uncertainties from statistics on profile, clinometry and dispersion mapping are 10–18 ppm.

5. Results

5.1. Component fitting

We fit 6 Voigt functions to the Sc $K\alpha$ profile, reported in table 4. A common Gaussian width, and a background amplitude were also included in the fitting function. The background was constant across the range observed. In principle a very small Compton tail and shelf can exist [24, 54], which would be discontinuous. Such a contribution is seen to be less than 15 counts. The uncertainties of the parameters are obtained from the diagonal covariance matrix. A plot with the data and fitted Voigts is shown in figure 7. All the literature has consistently seen evidence for six components in the spectra, as do we. Notice that the two smallest components are only 1.5% of the total spectral intensity, yet make a major contribution to the reduction of χ_r^2 in the fits. The spectrum is not well enough separated to justify any more than six spectral components i.e. they would not be able to be fitted due to correlations.

Theoretically it is known that we expect more components than six (actually many more) but these cannot be fitted empirically but require advanced atomic physics theory to investigate, which is one of the key reasons for obtaining this high-accuracy data set and calibration. In other words, we will be able to investigate this further with an advanced theoretical study in the future.

Table 4. Voigt profile component fit for Sc $K\alpha$. Numbers in parentheses are one standard error uncertainties. The common Gaussian width (σ) is 0.784(14) eV. Fitting uses initial estimates of independent parameters from [29]. Uncertainties are from fitting three independent scans.

Peak i	Centroid C_i eV	FWHM W_i eV	Fraction of integrated area	$E(K\alpha_{jk}) - E(K\alpha_{11})$ eV
$K\alpha_{11}$	4090.709(5)	1.15(7)	0.501(21)	0
$K\alpha_{12}$	4089.418(103)	2.89(41)	0.107(18)	-1.291
$K\alpha_{13}$	4087.752(89)	1.02(82)	0.015(6)	-2.957
$K\alpha_{15}$	4093.508(92)	2.01(22)	0.043(8)	+2.799
$K\alpha_{21}$	4085.918(16)	1.40(13)	0.321(15)	-4.791
$K\alpha_{22}$	4083.926(204)	3.86(92)	0.014(6)	-6.783

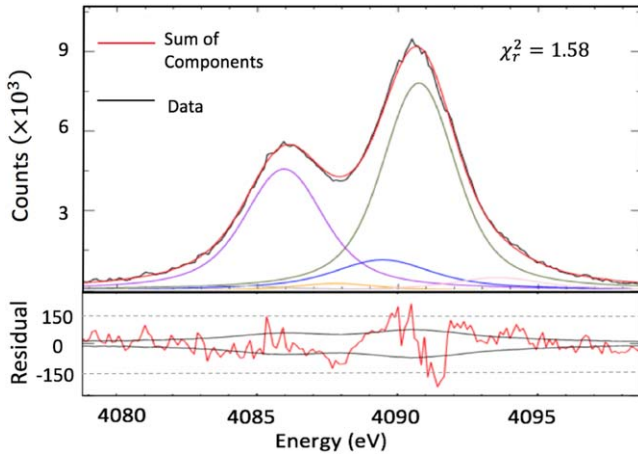


Figure 7. Fit of the six Voigt profiles for a single spectrum of Sc $K\alpha$. This corresponds with an intrinsic broadening of approximately 1 eV.

Table 5. Comparison of this work with Chantler *et al* [11, 29]. Differences are expressed in energy eV and as a fraction of the quadrature sum of the two 1σ uncertainties.

Peak i	Centroid difference, eV	Width difference, eV	Area difference
$K\alpha_{11}$	0	+0.02 (0.17 σ)	+0.002 (<0.05 σ)
$K\alpha_{12}$	-0.002 (<0.05 σ)	-0.24 (0.28 σ)	-0.002 (0.05 σ)
$K\alpha_{13}$	-0.006 (<0.05 σ)	+0.39 (0.22 σ)	-0.001 (0.07 σ)
$K\alpha_{15}$	+0.003 (<0.05 σ)	+0.08 (0.19 σ)	+0.005 (0.39 σ)
$K\alpha_{21}$	-0.013 (0.52 σ)	+0.13 (0.65 σ)	-0.001 (<0.05 σ)
$K\alpha_{22}$	+0.014 (<0.05 σ)	-0.37 (0.22 σ)	-0.005 (0.38 σ)

The differences between our characterisation and ones previously obtained from relative measurements [28, 29] are shown in tables 5 and 6. Comparisons are done after first shifting the previous literature’s profile such that the 2 $K\alpha_{11}$ centroids align. The comparisons are given in terms of absolute values, and as a fraction of the sum of the two 1σ uncertainties.

Since neither of those results were absolute measurements, they do not present energies for comparison and any subsequent fit would need to calibrate the energies separately, using at least two reference energies so that an energy or component characterisation would not ensue. This can be seen in table 4 compared with the $K\alpha_{11}$ component used to

Table 6. Comparison of this work with Anagnostopoulos *et al* [28]. Differences are expressed in energy eV and as a fraction of the quadrature sum of the two 1σ uncertainties. We present their component label, with our own in parentheses.

Label [28] (our label)	ΔE [28] see this work, eV (fraction of 1σ)
$K\alpha_{11}$	0
$K\alpha_{12}$ ($K\alpha_{15}$)	+0.016 (0.12 σ)
$K\alpha_{13}$ ($K\alpha_{12}$)	+0.088 (0.58 σ)
$K\alpha_{21}$	+0.004 (0.17 σ)
$K\alpha_{22}$ ($K\alpha_{13}$)	+0.341 (2.1 σ)
$K\alpha_{23}$ ($K\alpha_{22}$)	+0.043 (0.19 σ)

Table 7. Derived peak energies, widths, and amplitudes for Sc $K\alpha_1^0$ and $K\alpha_2^0$. Numbers in parentheses are one standard error uncertainties.

Peak i	Derived peak energy $K\alpha_i^0$, eV	FWHM W_i , eV	Proportion of integrated area
$K\alpha_1^0$	4090.699(10)	2.636(48)	0.665(9)
$K\alpha_2^0$	4085.926(18)	2.737(60)	0.335(15)

define the offset. Offsets are 0.036 eV [28, 29] and it is clear from the tables that there is also a slope inconsistency of 0.013 eV and circa 0.01 eV respectively over the range of the spectrum.

5.2. Derived peak position, eV

The derived peak positions (eV) for $K\alpha_1^0$ and $K\alpha_2^0$, averaged over all 9 scans, obtained from the full calibration set are shown in table 7 as the clean spectral peaks for ideal resolution, excluding Gaussian broadening. The instrumental (Gaussian) broadening shifts the derived peak location for $K\alpha_1^0$ and $K\alpha_2^0$ by -0.019 eV and +0.015 eV respectively as expected due to the dependence of the peak location on resolution. The uncertainties of the derived peaks also change, and increase by about a factor of 1.5 in each case: $K\alpha_1^0 = 4090.680(14)$ eV and $K\alpha_2^0 = 4085.941(29)$ eV. As expected, the uncertainty and characterisation become a more sensitive result of the variable broadening and they would be a more significant contribution to the transferable uncertainty.

These results are in excellent agreement with the previous experimental results [1]. However, this is not so surprising as Bearden reports a large uncertainty. A potential

Table 8. Comparison of derived peak energies for Sc $K\alpha_1^0$ and $K\alpha_2^0$ with experiment [1], and theory [13]. Numbers in parentheses are one standard error uncertainties.

Peak i	Measurement, eV	Difference, eV (as a sum of 1σ uncertainty)	References
$K\alpha_1^0$	4090.6(2)	-0.099 (0.47 σ)	[1]
$K\alpha_2^0$	4086.1(2)	+0.174 (0.80 σ)	
$K\alpha_1^0$	4090.15(42)	-0.549 (1.3 σ)	[13]
$K\alpha_2^0$	4085.43(44)	-0.496 (1.1 σ)	

discrepancy is seen compared with a previous theoretical calculation [13]. Our results for the peak energies are above those reported by Deslattes *et al*. The peak separation difference is ≈ 0.1 eV for both peaks. These differences are summarised in table 8. It is important to note again that the reference values for peak energies are not robust and transferable at the level we discuss and that the profile or component energies must be used for transfers. This table therefore illustrates some of the types of errors which can ensue accordingly. We also note that the discussion and characterisation of these issues, which was discussed experimentally and theoretically at the time [12, 13] has had much development of understanding of both experiment and theory in the intervening decades [11].

One issue plaguing modern atomic physics is the anomalous Z -dependence of the $K\alpha$ line intensities [22, 32, 33]. Our data for the proportion of integrated intensity yield $I(K\alpha_2): I(K\alpha_1)$ as 0.503(18). Three recent characterisations of the ratio of line intensities yield 0.525(4) [31], 0.52 [28], and 0.51(4) [29]. These are all larger than our value, but within our reported uncertainty. The observed pattern for elements $Z = 20$ to $Z = 80$ strongly suggests a ratio no greater than 0.51, as observed in this work. Our result is consistent and in line with the expected trend across the periodic table and the expected theoretical trend; however, two recent literature values express a significant anomaly with respect to this trend [28, 31], which may invite further investigation and anomalous line ratios even in recent measurements. The contribution by Ito *et al* [31] presents a characterisation of elements from Ca ($Z = 20$) to Ge ($Z = 32$). One anomaly in the publication is the line intensity ratio. Theory would predict an increasing ratio with Z , however there is no evidence of this in the values presented [31]. Indeed, their reported values for Sc and Ti are the two highest in the series, with three elements reported as having a transition probability below 0.5. This is likely part of the challenge and problem of multiple-component least-squares fitting.

6. Conclusion

Novel experimental techniques have been presented, and should be extended to investigations of anomalies in x-ray tests of QED. With similar analytical techniques, it may be possible to reach 1 ppm accuracy. This exciting avenue for

future work may reveal new physics. The approach to analysis for laboratory sources is effective, robust and portable. The approach for diagnosis and treatment of vignetting and also for the correlated uncertainties from reference characterisations and from the in-laboratory measurement and definition of the dispersion function is effective. This work shows the reliability of curved crystals in diffraction experiments for spectrometry. The error budget presented shows the robustness of the result to individual geometric uncertainties. Although the uncertainties particularly increase due to extrapolation and vignetting, these effects are isolated and constrained by the extensive data and calibration procedure. This work provides a high-accuracy absolute measurement of the Sc $K\alpha$ profile, component energies and parameters and the determined peak values Sc $K\alpha_1^0$, Sc $K\alpha_2^0$, filling a major gap in the current atomic physics literature, with standard error uncertainties of 2.4 and 4.4 ppm, some 20 times more accurate than the previous work. It compares results to past observations and measurements, and provides high-accuracy data towards the investigation of current challenges in x-ray characteristic radiation. The characterisation of 6 Voigt profiles is highly accurate and gives insight into asymmetries and the ratio of line intensities. The characterisation of component peaks is essential for transferability of standards and for detailed investigation of relativistic QM. We report the Sc $K\alpha$ energy to an accuracy consistent with current state-of-the-art measurements of other higher-energy spectra from higher- Z elements.

Appendix. Error analysis

An intrinsic precision and accuracy of a relative measurement and relative component uncertainties is given by the statistics accumulated in the spectrum and the resolution function or full width half maximum (fwhm) of the spectral profile. In this experiment, this is dominated by the integrated intensity in the $K\alpha_1$ or $K\alpha_2$ peaks (for Sc or the reference calibration lines) or in the $K\beta$ peaks for other reference calibration lines. Typically these spectra have been measured so that \sqrt{N} noise equates to a 0.004–0.008 eV (Sc) or 1–2 ppm uncertainty for the spectral peak energies e.g. $E(K\alpha_{1,0}^0)$ for each reference calibration line or peak, in each of three independent spectra at different offset angles from the Bragg position, and for each of three sets of clinometry data for each spectrum (figure 7). The statistics in the clinometry data are similar in count but narrower in distribution so represent a consistent statistical determination of angle to below this level. Indeed, the clinometry statistics are precise to 0.012 eV or 3 ppm for each spectrum and each clinometer set for scandium (9 data sets for Sc $K\alpha$). The standard error for the total data set $\sigma_{se} = \sqrt{\frac{1}{\sum_{i=1}^n \sigma_i^2}} \approx \frac{\sigma_i}{\sqrt{n}}$ is smaller than the standard deviation of each data set σ_i . The clinometry statistics give a standard error of 0.004 eV or 1 ppm.

Equally, the two dominant components, the $K\alpha_{11}$ and $K\alpha_{21}$ diagram lines, were determined to 2–7 ppm for each spectrum and for each file. Weak components, effectively

from satellite contributions, were naturally less well determined and dominated by both statistics and correlations between components as expected. The 3 scans for the Sc $K\alpha$ profile enable a standard error of order $\sqrt{3}$ smaller than the 1–4 ppm level. Hence yielding final standard errors in the fitting of the profile at the 2–4 ppm level.

If the uncertainty of profile energies from scans is significantly different, i.e. that the χ_r^2 would be greater than unity, then equation (A.1) can obtain the mean and standard error in the total Sc $K\alpha$ fitting statistic:

$$\bar{x} = \frac{\sum_{i=1}^n \frac{x_i}{\sigma_i^2}}{\sum_{i=1}^n \frac{1}{\sigma_i^2}}; \sigma_{se} = \sqrt{\frac{1}{(n-1) \sum_{i=1}^n \sigma_i^{-2}} \sum_{i=1}^n (x_i - \bar{x})^2} / \sigma_i^2. \quad (\text{A.1})$$

For x_i the energy of scan i , σ_i is the standard error in the energy of scan i as required.

The calibration spectra used references from the literature with uncertainties around the 1–3 ppm level. However, this is only relevant inasmuch as the dispersion function is stable and reproducible for the different spectra in off-axis positions, for the function of energy in terms of detector position, and for the function of angle or energy in terms of clinometry angle or voltage.

Important developments in technique and analysis have led to the three clinometers reporting consistent interpretations of the dispersion functions to remarkable accuracy, indeed to below 1 ppm or 0.004 eV in the region of Sc $K\alpha$. Critical in this was the approach to event mode of the spectral data to high count-rate, the optimisation of the resolution for the nearby calibration spectra, the collection of high statistics on the clinometry distributions, the novel dense set of calibration lines, and the processing and correction for vignettted profiles.

A key source of error in the experiment is the uncertainty in the fitting of the dispersion function, including all reference data, spectra, clinometry, theoretical spectral profiles and the consistency thereof.

The uncertainty is calculated using $\Delta f^2 = \Sigma Cov(X_i, X_j) \frac{df}{dX_i} \frac{df}{dX_j} \chi_r^2$, from the covariance matrix: $Cov(X_i, X_j) = E[X_i, X_j] - \mu_i \mu_j$ for for X_j one of the variables.

The uncertainty in figure 4 is the dashed line above and below the zero error residual line. Unsurprisingly, the uncertainty increases away from the three central calibration lines (Ti, V, Cr). The extrapolation to the Sc region increases the uncertainty further, by approximately a factor of three. This is optimised by having the ideal focus and resolution near Ti $K\alpha$, the nearest calibration reference spectra, and equally by having a larger set of Ti calibration spectra, closest to the Sc lines. The uncertainty of the fit for the dispersion function ($f_{disp}(V)$) at the Sc $K\alpha$ region is the uncertainty that propagates into the dispersion function in the *Mosplate* equation: $E = E_{mos}(X, f_{disp}(V))$. This accounts for the remainder of the uncertainty in the peak energies for the spectrum, namely 0.006 eV for $K\alpha_1^0$ and $K\alpha_2^0$.

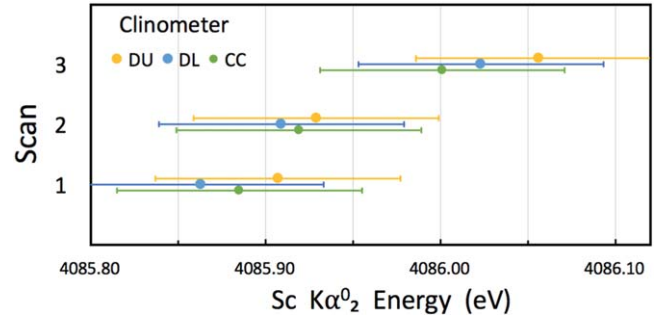


Figure A1. The values for the centroid of $K\alpha_2^0$ for each of the scans for each clinometer with its respective 1σ uncertainty without vignetting corrections.

Many systematics are assessed by comparing derived energies and fitting parameters for different spectra and different clinometers. In this experiment, all agree to within 1 standard error, or within 1–2 ppm. This explicitly includes the increased uncertainty due to the extrapolation, and implies that superior results should be obtainable for measurements by interpolation or e.g. for the determination of few-electron transitions and measurements of quantum electro-dynamics (the 1s Lamb shift in medium Z systems, for example).

There is an associated error or uncertainty for the vignetting function used. However, the vignetting function reduces χ_r^2 for all experimental spectra when compared to the current values in literature, and consistently improves agreement in the spectral determination for all data sets, so the error of this appears negligible and rather it reduces all uncertainties and systematics. The vignetting function is essential for experimental setups involving curved crystals, Seemann wedges and data that is ‘off-focus’. The vignetting function has been tested for each spectrum (for the narrow 2.14 mm wedge) and the results are self-consistent within the set of five elements. When the vignetting function is turned ‘off’ the dispersion function fits more poorly, and there is a greater spread in values for $K\alpha_1^0$ and $K\alpha_2^0$ for different scans and data sets (figure A1). Discrepancies and excursions occur in the vignettted profiles, so selecting a subset of non-vignettted profiles eliminates any systematic error or uncertainty from this source—and the results and uncertainties are indeed unaffected by adding or subtracting this subset. Indeed, depending on the side of the detector face that the scan is taken, a clear shift of energy is seen on the respective $K\alpha_1^0$ or $K\alpha_2^0$ line.

Upon correcting for vignetting the agreement of clinometers and spectral energy determinations is perhaps remarkable (figures 5, 6). These figures summarise the result and consistency from the uncertainties of all spectra, reference and scandium, for the derived peak positions and their stability for each clinometer. The agreement of all lies within 0.002 eV implying the the standard error from these sources will be smaller when pooled.

The greatest sources of uncertainty for this experiment are the scandium profile statistics, the extrapolation of the dispersion function from the region for Ti to Sc (figure 4), and the systematic uncertainties due to the uncertainties in the

geometric diffraction variables. Consider the effect of a geometric uncertainty (error) on the final measurement of a width, amplitude, component or derive peak energy of scandium $K\alpha$. Table 1 shows the values and uncertainty in each of the geometric parameters most relevant to the error in *Mosplate*. To arrive at an estimate for a one standard error uncertainty several sets of input parameters are computed and propagated through the analysis, where the parameters are set to their maximal or minimal values as allowed within their uncertainty. Overall, fourteen different sets of input data were used. This alters the three *Mosplate* functions, and importantly the equation: $\theta: E = E_{mos}(X, \theta)$. This uncertainty propagates through the dispersion function, when fixing the dispersion function and calculating for final energy, with the nine different sets of input, the centroid of energy for Sc $K\alpha_1^0$ and $K\alpha_2^0$ would vary at most by 0.009 eV and 0.011 eV respectively. Table 2 summarises the dominant statistical and systematic uncertainties and errors in our experiment.

Previous application of this detector and spectrometer technology to characterise the profile of Ti $K\beta$ [55] and V $K\beta$ [56] obtained very similar peak statistical uncertainty (1 ppm) and clinometer statistics. The total uncertainty from [56] is 1.3 ppm. However, the final uncertainties from both of those studies were dominated by the robustness of different data sets to 4.5 ppm and 2.7 ppm respectively, or approximately 0.022 eV or 0.015 eV respectively. Conversely in this study, because of the more advanced treatment of the dispersion function and vignetting, all calibration data sets and clinometer dispersion functions are stable and agree within one standard error. In particular, the different sets of wedge data and offset positions in the previous data sets gave significantly different results which we can now interpret to be due to vignetting, the stability of the dispersion function and the modelling of the wedge gaps. In the current investigation, the results for different wedge settings for Ti $K\alpha$ are all almost consistent, whereas for the earlier work the $K\beta$ wedges gave quite variable answers. Hence an additional systematic error source, although implicit in the robustness of the data sets of the earlier studies, can here be discussed explicitly in terms of the geometric and modelling uncertainties, which of course could be further improved with additional careful investigation.

When comparing the error budget presented here to that of Payne *et al* [37], there are a few key differences. The investigation into highly sensitive parameters of QED came with natural experimental difficulties. The statistics on the unknown helium-like spectra at a much lower count-rate, is some 6 ppm in that study whereas it is quite straightforward to obtain a statistical uncertainty for Sc $K\alpha_1$ or $K\alpha_2$ of 2–3 ppm. The unknown helium-like clinometry statistical uncertainty was 9.7 ppm with a calibration clinometry uncertainty of 7.3 ppm, as compared to the current 1.0 ppm and 1.7 ppm respectively. This is particularly due to an increased event-mode-like clinometry data collection which also collects data at a higher frequency. Uncertainties from shot noise, background and the unknown r-line width are negligible or do not exist in the current experiment, but were significant in the

helium-like QED experiment on Ti^{20+} . That detector type used a circular aperture yielding potentially significant ‘detector corrections’/uncertainties of 5.1 ppm including in the ‘detector fit’, compared to an almost negligible uncertainty from all geometric causes in the current experiment [50]. Hence we are able to report an uncertainty of almost an order of magnitude lower than this other experiment.

A great advantage of curved crystal measurement compared with many single or double flat crystal geometries for high accuracy measurement is that any small uncertainty in source or detector location at the micron level leads to shifts in the detection location and often interpreted absolute energy of much larger magnitudes.

An additional major benefit in using the backgammon detector is that it reduces one of the greatest uncertainties of many similar investigations using CCDs or other pixel detectors. The pixel resolution is not a systematic uncertainty for this experiment, as the backgammon detector records a continuum, or analogue, of data points, whereas pixel detectors are limited by their pixel size.

Further advantages of backgammon detectors over pixel based ones include improved energy/flux linearity, and greater damage resistance from x-rays [50]. A further improvement is that our set-up is in a near vacuum state, whereas Mendenhall *et al* perform experiments where air absorption is not negligible. Their statistical quality is extremely high (0.05 ppm), though compiled from spectra which do not cover the same energy range, in part to characterise these systematics. Their dependence on temperature and related components have very little effect or uncertainty in our data. Their final quoted uncertainty is 0.13 ppm, dominated by temperature, counting and angle. Our angle uncertainty is given effectively by the dispersion function, so is larger but also dependent upon the statistical data collection of the angular variables.

ORCID iDs

C T Chantler  <https://orcid.org/0000-0001-6608-0048>

References

- [1] Bearden J A 1967 X-ray wavelengths *Rev. Mod. Phys.* **39** 78–124
- [2] Melia H A, Chantler C T, Smale L F and Illig A J 2019 The characteristic radiation of copper $K\alpha_{1,2,3,4}$ *Acta Crystallogr. A* **75** 527–40
- [3] Moseley H 1913 The high-frequency spectra of the elements *Phil. Mag.* **16** 1024–34
- [4] Allison S K 1933 The natural widths of the $K\alpha$ x-ray doublet from 26Fe to 47Ag *Phys. Rev.* **44** 63–72
- [5] Williams E J 1934 Anomalous dispersion and absorption of x-rays *Proc. R. Soc. A* **143** 358–76
- [6] Hänsch T W, Alnis J, Fendel P, Fischer M, Gohle C, Herrman M, Holzwarth R, Kolachevsky N, Udem T and Zimmermann M 2005 Precision spectroscopy of hydrogen and femtosecond laser frequency combs *Phil. Trans. R. Soc. A* **363** 2155

- [7] Pohl R *et al* 2010 The size of the proton *Nature* **466** 213–7
- [8] Chantler C T *et al* 2012 Testing three-body quantum electrodynamic with trapped Ti^{20+} ions: evidence for a Z-dependent divergence between experiment and calculation *Phys. Rev. Lett.* **109** 153001
- [9] Antognini A *et al* 2013 Proton structure from the measurement of 2s–2p transition frequencies of muonic hydrogen *Science* **339** 417–20
- [10] Pohl R, Nez F, Fernandes L M P, Amaro F, Biraben F, Cardoso J M R, Covita D S, Dax A, Dhawan S and Diepold M 2016 Laser spectroscopy of muonic deuterium *Science* **353** 669–73
- [11] Chantler C T, Smale L F and Hudson L T 2019 X-ray energies *International tables for Crystallography* ed R Welberry vol C (Dordrecht: Kluwer Academic Publishers) p 4.2.2.1 ch 4. 2.2
- [12] Deslattes R D, Kessler E G Jr, Indelicato P and Lindroth E 1999 X-ray wavelengths *International tables for Crystallography* ed A J C Wilson and E Prince vol C (Dordrecht: Kluwer Academic Publishers) pp 200–13
- [13] Deslattes R D, Kessler E G, Indelicato P, de Billy L, Lindroth E and Anton J 2003 X-ray transition energies: new approach to a comprehensive evaluation *Rev. Mod. Phys.* **75** 35–99
- [14] Vovna V I, Domashevskaya E P and Okotrub A V 2017 X-ray and x-ray electron spectroscopy of new materials *J. Struct. Chem.* **58** 1057–60
- [15] Chantler C T, Lowe J A and Grant I P 2010 Multiconfiguration dirac-fock calculations in open-shell atoms: convergence methods and satellite spectra of the copper $K\alpha$ photoemission spectrum *Phys. Rev. A* **82** 052505
- [16] Hansen S B *et al* 2005 Temperature determination using $k\alpha$ spectra from *m*-shell ti ions *Phys. Rev. E* **72** 036408
- [17] Armelao L, Bottaro G, Pascolini M, Sessolo M, Tondello E, Bettinelli M and Speghini A 2008 Structure luminescence correlations in europium-doped sol gel zno nanopowders *J. Phys. Chem. C* **112** 4049–54
- [18] Uo M, Wada T and Sugiyama T 2015 Applications of x-ray fluorescence analysis (xrf) to dental and medical specimens *Japan. Dental Sci. Rev.* **51** 2–9
- [19] Smale L F, Chantler C T and Kimpton J A 2015 Methodology for the characterisation of characteristic spectral profiles, applied to chromium $K\alpha$ *X-Ray Spectrom.* **44** 54–62
- [20] Gillaspay J D, Chantler C T, Paterson D, Hudson L T, Serpa F G and Takcs E 2010 First measurement of Lyman alpha x-ray lines in hydrogen-like vanadium: results and implications for precision wavelength metrology and tests of QED *J. Phys. B: At. Mol. Opt. Phys.* **43** 074021
- [21] Indelicato P and Lindroth E 1992 Relativistic effects, correlation, and QED corrections on $K\alpha$ transitions in medium to very heavy atoms *Phys. Rev. A* **46** 2426–36
- [22] Hölzer G, Fritsch M, Deutsch M, Härtwig J and Förster E 1997 $K\alpha_{1,2}$ and $K\beta_{1,3}$ x-ray emission lines of the 3d transition metals *Phys. Rev. A* **56** 4554–68
- [23] Mendenhall M H, Henins A, Hudson L T, Szabo C I, Windover D and Cline J P 2017 High-precision measurement of the x-ray Cu $K\alpha$ spectrum *J. Phys. B: At. Mol. Opt. Phys.* **50** 1–18
- [24] Illig A J, Chantler C T and Payne A T 2013 Voigt profile characterization of copper $K\alpha$ *J. Phys. B: At. Mol. Opt. Phys.* **46** 235001
- [25] Lowe J A, Chantler C T and Grant I P 2010 A new approach to relativistic multi-configuration quantum mechanics in titanium *Phys. Lett. A* **374** 4756–60
- [26] Lowe J A, Chantler C T and Grant I P 2011 *Ab initio* determination of satellite intensities in transition-metal photoemission spectroscopy using a multiconfiguration framework *Phys. Rev. A* **83** 060501
- [27] Kawai J, Nakamura E, Nihei Y, Fujisawa K and Gohshi Y 1990 Sc $K\alpha$, and $K\alpha$ x-ray fluorescence spectra *Spectrochim. Acta B* **45** 463–79
- [28] Anagnostopoulos D, Sharon R, Gotta D and Deutsch M 1999 $K\alpha$ and Kx -ray emission spectra of metallic scandium *Phys. Rev. A* **60** 2018–33
- [29] Chantler C T, Kinnane M N, Su C and Kimpton J A 2006 Characterization of $K\alpha$ spectral profiles for vanadium, component redetermination for scandium, titanium, chromium, and manganese, and development of satellite structure for $Z = 21$ to $Z = 25$ *Phys. Rev. A* **73** 012508
- [30] Limandri S P, Bonetto R D, Carreras A C and Trincavelli J C 2010 $K\alpha$ satellite transitions in elements with $12 < Z < 30$ produced by electron incidence *Phys. Rev. A* **82** 032505
- [31] Ito Y *et al* 2016 $K\alpha_{1,2}$ x-ray linewidths, asymmetry indices, and [KM] shake probabilities in elements Ca to Ge and comparison with theory for Ca, Ti, and Ge *Phys. Rev. A* **94** 042506
- [32] Salem S I and Lee P L 1976 Experimental widths of *K* and *L* x-ray lines *At. Data Nucl. Data Tables* **18** 233–41
- [33] McCrary J H, Singman L V, Ziegler L H, Looney L D, Edmonds C M and Harris C E 1971 *K*-fluorescent-x-ray relative-intensity measurements *Phys. Rev. A* **4** 1745–50
- [34] Sorum H 1987 The *K* x-ray spectra of the 3d transition metals Cr, Fe, Co, Ni and Cu *J. Phys. F: Met. Phys.* **17** 417
- [35] Parratt L G 1959 Electronic band structure of solids by x-ray spectroscopy *Rev. Mod. Phys.* **31** 616–45
- [36] Chantler C T, Lowe J A and Grant I P 2013 High-accuracy reconstruction of titanium x-ray emission spectra, including relative intensities, asymmetry and satellites, and *ab initio* determination of shake magnitudes for transition metals *J. Phys. B: At. Mol. Opt. Phys.* **46** 015002
- [37] Payne A T, Chantler C T, Kinnane M N, Gillaspay J D, Hudson L T, Smale L F, Henins A, Kimpton J A and Takacs E 2014 Helium-like titanium x-ray spectrum as a probe of QED computation *J. Phys. B: At. Mol. Opt. Phys.* **47** 185001
- [38] Deslattes R D and Kessler E G Jr 1985 Experimental evaluation of inner-vacancy level energies for comparison with theory *Atomic Inner-Shell Physics* ed B Crasemann (New York: Plenum) pp 181–235
- [39] Deslattes R D and Henins A 1973 X-Ray to visible wavelength ratios *Phys. Rev. Lett.* **31** 972–5
- [40] Kessler E G Jr, Owens S M, Henins A and Deslattes R D 1999 Silicon lattice comparisons related to the Avogadro project: uniformity of new material and surface preparation effects *IEEE Trans. Instrum. Meas.* **48** 221–4
- [41] Briand J P, Indelicato P, Simionovici A, Vicente V S, Liesen D and Dietrich D 1989 Spectroscopic study of hydrogenlike and heliumlike xenon ions *Europhys. Lett.* **9** 225–30
- [42] Beyer H F *et al* 1993 X-ray transitions associated with electron-capture into bare dysprosium *J. Phys. B: At. Mol. Opt. Phys.* **26** 1557–67
- [43] Pham T L, Nguyen T V, Lowe J A, Grant I P and Chantler C T 2016 Characterization of the copper $k\beta$ x-ray emission profile: an *ab initio* multi-configuration dirachartreefock approach with bayesian constraints *J. Phys. B: At. Mol. Opt. Phys.* **49** 035601
- [44] Kimpton J A, Kinnane M N and Chantler C T 2006 Development of backgammon-type multiwire proportional counters for the detection of x rays *Rev. Sci. Instrum.* **77** 083102
- [45] Allemand R and Thomas G 1976 Nouveau detecteur de localisation: Le dispositif a jeu de jacquet *Nucl. Instrum. Methods* **137** 141–9
- [46] Smith G C 1984 High accuracy gaseous x-ray detectors *Nucl. Instrum. Methods Phys. Res.* **222** 230–7

- [47] Smith G C, Fischer J and Radeka V 1984 Resolution for x-rays in gas proportional chambers *IEEE Trans. Nucl. Sci.* **111–5** NS-31
- [48] Duval B, Barth J, Deslattes R, Henins A and Luther G 1984 Position-sensitive x-ray detector *Nucl. Instrum. Methods Phys. Res.* **222** 274–8
- [49] Mizogawa T, Sato M and Awaya Y 1995 Application of the MBWC two-dimensional position readout technique to a multiwire proportional counter *Nucl. Instrum. Methods Phys. Res. A* **366** 129–36
- [50] Melia H A, Dean J W, Smale L F, Illig A J and Chantler C T 2019 Count-rate, linearity and performance of new backgammon detector technology *X-Ray Spectrom.* **48** 218–31
- [51] Chantler C T 1991 X-ray diffraction of bent crystals in bragg geometry: I. Perfect crystal modelling *J. Appl. Crystallogr.* **25** 674–93
- [52] Chantler C T 1991 X-ray diffraction of bent crystals in bragg geometry: II. Non-ideally imperfect crystals, modelling and results *J. Appl. Crystallogr.* **25** 694–713
- [53] Paterson D, Chantler C T, Tran C Q, Hudson L T, Serpa F G and Deslattes R D 1997 Absolute calibration of an x-ray spectrometer on the NIST electron-beam ion trap: control, design and systematics *Phys. Scr.* **1997** 400
- [54] Enkisch H, Sternemann C, Paulus M, Volmer M and Schülke W 2004 3d spectator hole satellites of the Cu $K\beta_{1,3}$ and $K\beta_{2,5}$ emission spectra *Phys. Rev. A* **70** 022508
- [55] Chantler C T, Smale L F, Kimpton J A, Crosby D N, Kinnane M N and Illig A J 2013 Characterization of the titanium $K\beta$ spectral profile *J. Phys. B: At. Mol. Opt. Phys.* **46** 145601
- [56] Smale L F, Chantler C T, Kinnane M N, Kimpton J A and Crosby D N 2013 Characterization of the $K\beta$ spectral profile for vanadium *Phys. Rev. A* **87** 022512